

Preparation, Crystal Structure, Magnetic and Electronic Properties of Ternary Rare-Earth Nitrides of Indium (R_3N)In

Martin Kirchner, Rainer Niewa, Walter Schnelle, Frank R. Wagner and R. Kniep

For a couple of years ternary nitrides of the general formula $(Ca_3N)M$ are known [1-3]. The compounds crystallize in a cubic anti-perovskite type structure (see Fig. 1) and exhibit interesting features concerning the electronic situation. Assuming nitrogen and calcium to form ions N^{3-} and Ca^{2+} , respectively, one can achieve – within the same structure type – various electronic configurations: from an electron excess as in $(Ca_3N)Au$ (formally $(Ca^{2+})_3N^{3-}Au^- 2e^-$) [1], via compounds $(Ca_3N)M$ ($M = P^{3-}, As^{3-}, Sb^{3-}, Bi^{3-}$) [2], which obey the octet rule, to an electron deficiency as in $(Ca_3N)Tl$ ($(Ca^{2+})_3N^{3-}Tl^{3-}$) [3] or $(Ca_3N)M$ ($M = Ge, Sn, Pb$) [2]. This change in the electronic situation is mirrored in the physical behavior of the compounds: $(Ca_3N)Au$ represents an electronic conductor, the pentel compounds are insulators ($M = P, As$) or semiconductors ($M = Sb, Bi$), whereas the electron deficient compounds are again electric conductors. Meanwhile, little information about ternary nitrides with the formula $(R_3N)In$ ($R =$ rare-earth metal) is available [4], although $(La_3N)In$ and $(Nd_3N)In$ have already been reported [5, 6]. In such rare-earth metal compounds the valence electron concentration might be adjustable by the nitrogen content in the sense of $(R_3N_{1-x})In$ within large ranges. The synthesis of these compounds provides new data-material to shed light upon the question of metal-metal bonding. The host compounds R_3In ($AuCu_3$ -structure type) are only known for the lighter rare-earth metals La, Ce, Pr, Nd and Sm [7, 8]. Due to stabilization it is possible to obtain the cubic perovskite compounds $(R_3C)In$ [9] even with the heavier rare-earth metals up to Lu.

In several studies, mainly on carbides $(R_3C)M$ [9] ($M =$ main group metal), the crystal structure for compounds of this formula type is observed to be of the cubic anti-perovskite type. The disordered fcc packing of R and M can be unambiguously distinguished from the ordered arrangement only for element combinations R/M with sufficiently different numbers of electrons by powder X-ray diffraction methods (XRD). Especially for $(Ce_3N)In$ this problem becomes apparent since the binary compound Ce_3In is known to occur in both crystal

structures, ordered $AuCu_3$ type and disordered fcc, depending on the heat treatment during synthesis [10]. For $(Ce_3N)In$ the ordered arrangement of metal atoms produces weak reflections in the powder XRD diagram which are not allowed for a disordered structure with an F -centered unit cell. Information on the degree of a possible Ce-In disorder and on the crystallographic position and occupancy of N was unambiguously extracted from neutron powder diffraction on a $(Ce_3N)In$ sample. The results from Rietveld refinements clearly show that $(Ce_3N)In$ crystallizes in the cubic anti-perovskite structure type with Ce and In arranged in an ordered cubic close packing and N occupying exclusively the octahedral holes formed by Ce. An analogous description is based on all vertex-sharing octahedra $NCe_{6/2}$ of the ReO_3 -type incorporating In within the large cuboctahedral voids formed by Ce. The nitrogen content determined from the Rietveld refinement ($Ce_3InN_{0.92(1)}$) is in good agreement with the composition derived from chemical analyses ($Ce_3InN_{0.91(2)}O_{0.05(1)}$). These data indicate the possibility of occupancies below unity

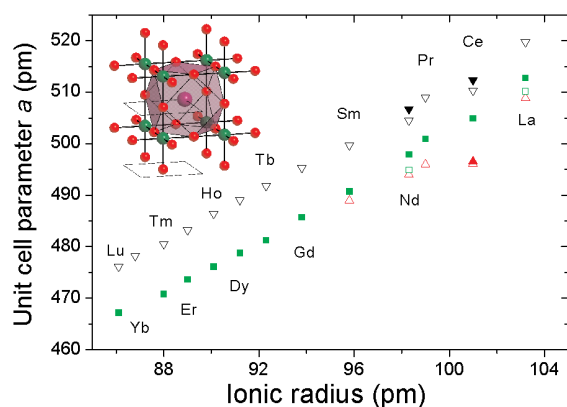


Fig. 1: Lattice parameter of the cubic compounds $(R_3[])In$ (red triangles) [7, 8], $(R_3C)In$ (black turned triangles) [9], $(R_3N)In$ (green squares) [5, 6] ($R =$ rare-earth element, values obtained in this study: solid symbols, literature values: open symbols) plotted against the ionic radius of the rare-earth metal for six-fold coordination. Inset: Anti-perovskite structure of the compounds $(R_3X)In$ ($X = [], C, N$), In: violet, R: red, X: green.

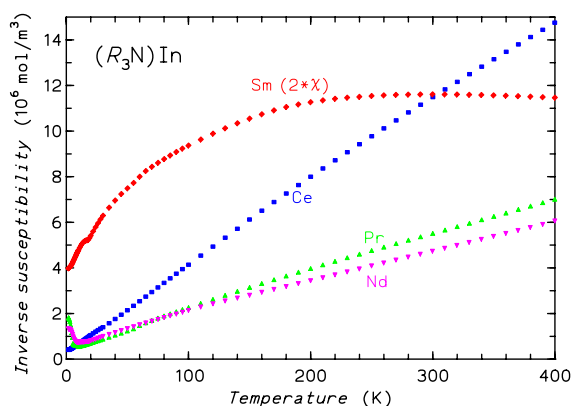


Fig. 2: Inverse magnetic susceptibility of $(\text{Ce}_3\text{N})\text{In}$ (blue squares), $(\text{Pr}_3\text{N})\text{In}$ (green triangles), $(\text{Nd}_3\text{N})\text{In}$ (magenta turned triangles) and $(\text{Sm}_3\text{N})\text{In}$ (red diamonds) as a function of the temperature T .

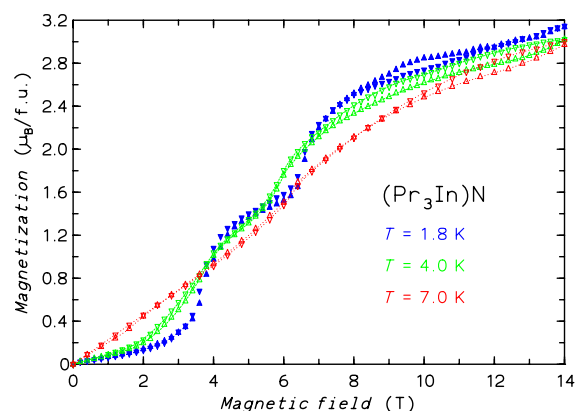


Fig. 3: Isothermal magnetization curves for polycrystalline $(\text{Pr}_3\text{N})\text{In}$ at different temperatures (blue: 1.8 K, green: 4.0 K, red: 7.0 K) showing metamagnetic transitions (triangles: increasing field, turned triangles: decreasing field).

for the octahedral site, interchangeability of N and O and a structure-determining influence of N in the sense of an induction of local order around nitrogen.

For all rare-earth metals except Eu and Yb a compound $(R_3\text{N})\text{In}$ was obtained exhibiting the cubic perovskite structure. Figure 1 shows the lattice parameter of these compounds $(R_3\text{N})\text{In}$ together with those of the respective carbides $(R_3\text{C})\text{In}$ [9] as a function of the ionic radius of the rare-earth element. The approximately linear dependence within each series is evident. For comparison the binary compounds $(R_3\text{In})$ [7, 8] ($R = \text{La}, \text{Ce}, \text{Pr}, \text{Nd}, \text{Sm}$) are also included. The heavier rare-earth metals ($R = \text{Gd} - \text{Lu}$) do not form the phase $(R_3\text{In})$, but N and C are able to stabilize the $(R_3\text{In})$ substructure even for the smallest rare-earth elements. Compared to the binaries, nitrogen causes a less strong expansion of the substructure than carbon. This could be attributed to the fact that a formal N^{3-} -ion is smaller than a formal C^{4-} -ion in the crystal. A closer inspection of the lattice parameters shows two anomalies: the lattice parameter of Ce_3In strongly deviates to lower values. We obtain a lattice parameter of 496.6(8) pm which confirms those reported previously (496.1 pm) [10]. Ce_3In is reported to be a heavy fermion system [11] and our susceptibility data ($\mu_{\text{eff}} = 2.58 \mu_{\text{B}}/\text{Ce-atom}$) are consistent with a pure $\text{Ce}(4f^1)$ state. Thus, this deviation remains unexplained. Concerning the carbides we obtained lattice parameters for $(\text{Ce}_3\text{C})\text{In}$ and $(\text{Nd}_3\text{C})\text{In}$ fitting better to those of the

other ternary carbides from literature [12, 13]. The reason for the difference might be an occupation of the metalloid site below unity in the previous investigations.

The magnetic properties of the $(R_3\text{N})\text{In}$ compounds are dominated by the magnetic moment of the rare-earth element R . $(\text{La}_3\text{N})\text{In}$ is slightly diamagnetic at room temperature with the susceptibility rising towards lower temperatures due to minor paramagnetic impurities. A fit yields $\chi_0 \downarrow -10 \times 10^{-6}$ emu/mol (-1.3×10^{-10} m³/mol). Thus, $(\text{La}_3\text{N})\text{In}$ is a Pauli-paramagnet with $\chi_{\text{P}} \uparrow +80 \times 10^{-6}$ emu/mol (1.0×10^{-9} m³/mol). This corresponds to an electronic density of states of 2.5 states/eV (per formula unit, 2 spin directions) at the Fermi level within the model of free electrons.

Above 50 K $(\text{Ce}_3\text{N})\text{In}$ and $(\text{Pr}_3\text{N})\text{In}$ display a behavior approximately in accordance with a Curie-Weiss law. However, there is curvature due to crystal field effects (Fig. 2). A fit to a Curie-Weiss law at high temperatures yields an effective magnetic moment of $\mu_{\text{eff}} = 2.53 \mu_{\text{B}}/\text{Ce-atom}$. From the lattice parameter (see Fig. 1) and from X-ray absorption spectroscopy (XAS, see below) there is no indication for any deviation from the $4f^1$ state of Ce. At low temperatures $(\text{Ce}_3\text{N})\text{In}$ orders antiferromagnetically as is indicated by a kink in $\chi(T)$ at $T_{\text{N}} = 9$ K. A second kink at 7 K might be due to a rearrangement of the spin structure. The low-temperature magnetic structure was investigated by powder neutron scattering and leads to a simple $\mathbf{k}_{\text{mag}} = 1/2 \ 1/2 \ 1/2$ spin arrangement. $(\text{Pr}_3\text{N})\text{In}$ con-

tains only $\text{Pr}(4f^2)$ species and orders antiferromagnetically ($T_N = 11$ K). Interestingly, the compound displays a rich magnetic phase diagram as can be seen from two metamagnetic transitions (see Fig. 3). $(\text{Nd}_3\text{N})\text{In}$ orders antiferromagnetically at $\dagger 10$ K.

The susceptibility of $(\text{Sm}_3\text{N})\text{In}$ does not obey the Curie-Weiss law due to the low-lying excitations involving the $^6\text{H}_{5/2}$ and $^6\text{H}_{7/2}$ multiplets typical for $\text{Sm}(4f^2)$. A small cusp at 17.5(1.0) K in $H_{\text{ext}} = 10$ kOe ($B_{\text{ext}} = 1.0$ T) indicates antiferromagnetic order of the $\text{Sm}(4f^5)$ ions in this compound.

For independent information on the electronic state of the rare-earth elements we measured XAS spectra at the R - L_{III} threshold. The applied range of photon energy makes it possible to measure in transmission geometry and thus to obtain data of the bulk material less obscured by surface impurities. Figure 4a shows the Sm - L_{III} edge of $(\text{Sm}_3\text{N})\text{In}$ together with the spectrum of $\text{Sm}_2^{\text{III}}\text{O}_3$ as a reference. Clearly, the positions of the absorption edges coincide in energy indicating an identical oxidation state for Sm in both compounds. A contribution of $\text{Sm}(4f^6)$ would be expected at about 7 eV lower in energy. Unlike such compounds as, e. g., $\text{Sm}(4f^6)$, $\text{Sm}(4f^5)$ or $\text{Ce}(4f^1)$ with a single peak structure in the R - L_{III} XAS spectra, the R - L_{III} XAS spectrum of $\text{Ce}(4f^0)$ compounds exhibits two maxima as shown for $\text{Ce}^{\text{IV}}\text{O}_2$. Fig. 4b compares the Ce - L_{III} XAS spectrum of $(\text{Ce}_3\text{N})\text{In}$ with the single peak spectrum of $\text{Ce}^{\text{III}}\text{F}_3$ and the double peak spectrum of $\text{Ce}^{\text{IV}}\text{O}_2$. It can be seen that the spectrum of $(\text{Ce}_3\text{N})\text{In}$ does not only display a single peak but also the signal maximum coincides with that of the spectrum of $\text{Ce}^{\text{III}}\text{F}_3$.

Both facts indicating a pure $\text{Ce}(4f^1)$ state in $(\text{Ce}_3\text{N})\text{In}$. In order to elucidate some principle features of the electronic structure of the isostructural $(R_3\text{N})\text{In}$ compounds we performed scalar relativistic LDA band structure calculations for the prototype La compounds $(\text{La}_3\text{N})\text{In}$ and La_3In using the TB-LMTO-ASA method.

The total electronic density of states (DOS) for $(\text{La}_3\text{N})\text{In}$ in the region from -6 eV to 0 eV below the Fermi level (E_F) roughly exhibits two groups separated by a pseudo-gap (Fig. 5a). The lower lying group (-5.9 eV to -2.4 eV) consists of two independent but slightly overlapping features: i) a single peak structure (-5.9 eV to -4.3 eV) originating from a nearly pure $\text{In}(5s)$ band which does not mix with $\text{N}(2p)$ bands and only very slightly with $\text{La}(5d, 6s)$ bands, and ii) an ‘‘u-shaped’’ feature (-5.0 eV to -2.4 eV) consisting of three $\text{N}(2p)$ majority bands mixing slightly with $\text{La}(5d)$ states. This group of electronic states (together with the low-lying single peak structure from one $\text{N}(2s)$ band) represents a typical semiconductor/insulator-type band filling of a predominantly ionic solid: All majority band states are completely filled leading to a nitrogen species with filled $2s2p$ subshells (formal N^{3-}) and an In species with a filled $5s$ subshell. The second group of electronic states consisting of $\text{In}(5p)$ and $\text{La}(5d)$ majority bands starts just where the first one ends at -2.4 eV and can be regarded to be responsible for metal-metal bonding. This leads to partially filled $\text{In}(5p)$, $\text{La}(5d)$ subshells and metallic properties of the compound.

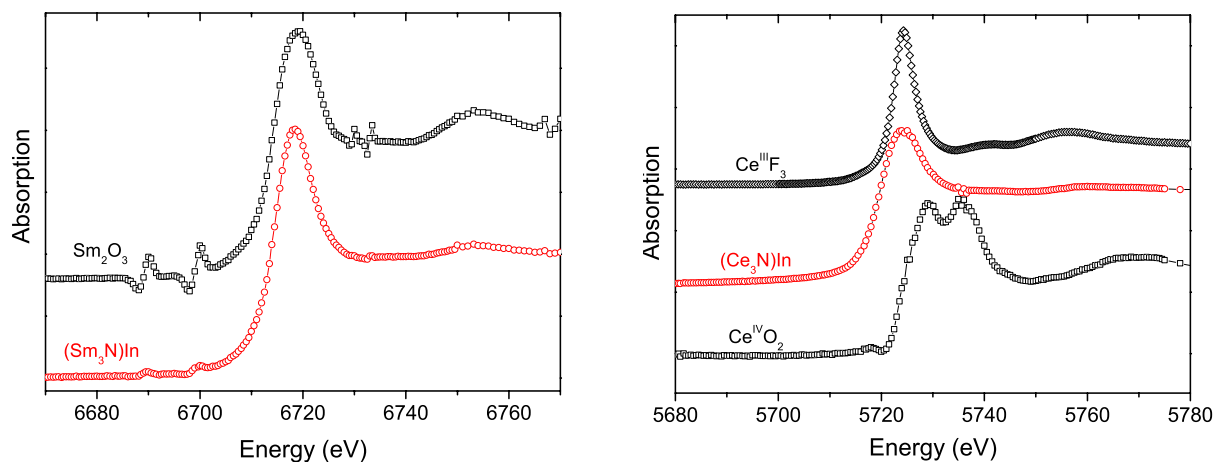


Fig. 4: XAS spectra at the R - L_{III} edge of a) $(\text{Sm}_3\text{N})\text{In}$ and Sm_2O_3 for comparison, b) $(\text{Ce}_3\text{N})\text{In}$, CeF_3 and CeO_2 for comparison.

The total DOS at the Fermi level $N(E_F) = 2.6$ states/eV cell is in agreement with the value derived from Pauli-paramagnetic contributions (see above) to $\chi(T)$.

In order to further characterize chemical bonding in this DOS picture we calculated energy-resolved Crystal Orbital Hamiltonian Populations (COHP) [14] for the significant interatomic two-center orbital interactions. For the total orbital interactions La–N (Fig. 6a) all the $N(2p)$ projected DOS below E_F exhibits a La–N bonding characteristic while above E_F they are all antibonding. In connection with the DOS analysis this gives a picture of partially covalent La–N interactions which is typically expected between La cations and formal N^{3-} anions. Two-center orbital interactions involving homoatomic interactions In–In are small due to large distances $d(\text{In–In}) = 513$ pm. The position of E_F within this COHP(E) curve is similar to that for the Bi–Bi COHP(E) in $(\text{Ca}_3\text{N})\text{Bi}$: the large antibonding peak lies just below E_F , while for $(\text{Ca}_3\text{N})\text{Tl}$ it lies just above [3]. One might conclude that In and Bi in the respective compounds have a similar electronic population, i.e., In is quite electron-rich. However, in contrast to the situation for $(\text{Ca}_3\text{N})\text{Bi}$, occupied $\text{In}(5p)$ bands are strongly involved in metal-metal interactions which makes a majority band assignment impossible: $\text{In}(5p)$ bands are strongly mixing with $\text{La}(5d)$ bands. The two-center In–La orbital interactions are sizable and numerous (each In atom has 12 La neighbors) and they exhibit an electronically optimized behavior, the Fermi energy just separating the bonding from the antibonding interactions. Therefore, In behaves as a species with an electronic octet, however, it shows large amounts of covalent mixing with $\text{La}(5d)$ states, with the result that even a formal electronic population cannot be safely derived from these considerations. Large two-center orbital interactions La–La can be seen in the COHP(E) curve. Among the strong orbital interactions they are the only ones which are not at maximum at E_F but increase further beyond.

Summarizing our results for $(\text{La}_3\text{N})\text{In}$ in a more chemically sound conclusion we observe ionic $\text{NLa}_{6/2}$ octahedra with formal N^{3-} central ions showing some covalent bonding with the La ions embedded in a framework of mutually strongly interacting metal atoms' orbitals, where only the homoatomic In–In orbital interactions are weak (“ionic polyhedron embedded in metallic matrix”).

If the central N atom of the ionic polyhedron is removed leading to the compound La_3In the electronic structure changes smoothly: the $N(2p)$ majority bands just disappear in the lower-lying DOS group and only the $\text{In}(5s)$ peak remains there (Fig. 5b). Furthermore, since only an N atom has been removed and not an N^{3-} with six p electrons, the higher-lying DOS structure encloses three additional electrons and $1\frac{1}{2}$ bands are now additionally available for metal-metal bonding. The question arises in which interaction these get employed. The

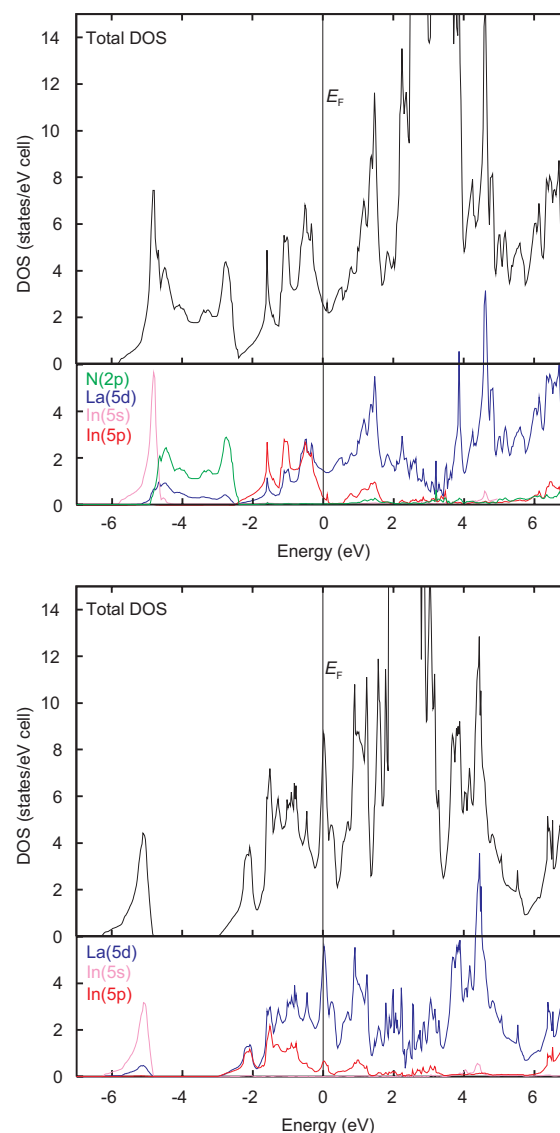


Fig. 5: DOS of a) $(\text{La}_3\text{N})\text{In}$: total DOS (black), $N(2p)$ projection (green), $\text{La}(5d)$ projection (blue), $\text{In}(5s)$ projection (pink), $\text{In}(5p)$ projection (red), b) La_3In : total DOS (black), $\text{La}(5d)$ projection (blue), $\text{In}(5s)$ projection (pink) and $\text{In}(5p)$ projection (red).

COHP(E) (Fig. 6b) curves give the unique answer: While orbital interactions In–La nearly remain at their maximum, the La–La orbital interactions gain bonding contributions. This can be easily seen comparing the fraction of occupancy of the bonding part (between about -3 eV and $+3$ eV) of the

COHP(E) curve for both compounds. This change in the bonding situation can be experimentally observed by a dramatic change of the mechanical properties: $(\text{La}_3\text{N})\text{In}$ is brittle while La_3In is ductile and extremely hard.

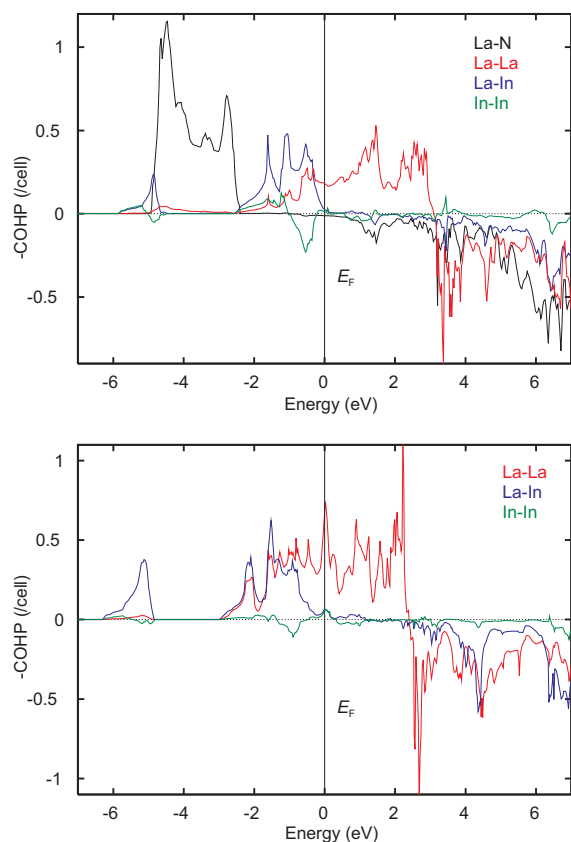


Fig. 6: COHP(E) diagrams of a) $(\text{La}_3\text{N})\text{In}$: La–N (black), La–La (red), La–In (blue), and In–In (green), b) La_3In : La–La (red), La–In (blue), and In–In (green).

References

- [1] J. Jäger, D. Stahl, P. C. Schmidt, and R. Kniep, *Angew. Chem.* **105**, 738 (1993), *Angew. Chem. Int. Ed.* **32**, 709 (1993).
- [2] M. Y. Chern, D. A. Vennos, F. J. DiSalvo, *J. Solid State Chem.* **96**, 415 (1992).
- [3] R. Niewa, W. Schnelle, F. R. Wagner, *Z. Anorg. Allg. Chem.* **627**, 365 (2000).
- [4] M. Kirchner, Diplomarbeit, Jena 2001.
- [5] J.-T. Zhao, Z.-C. Dong, J. T. Vaughey, J. E. Ostenson, J. D. Corbett, *J. Alloys Comp.* **230**, 1 (1995).
- [6] H. Haschke, H. Nowotny, F. Benesovsk, *Monatsh. Chem.* **98**, 2157 (1967).
- [7] S. P. Delfino, S. A. Saccone, R. Ferro, *J. Alloys Comp.* **102**, 289 (1984).
- [8] Yatsenko, A. A. Semyannikov, H. O. Shkarov, E. G. Fedorova, *J. Less-Common Met.* **90**, 95 (1983).
- [9] T. M., Gesing, K. H. Wachtmann, W. Jeitschko, *Z. Naturforsch.* **52b**, 176 (1997).
- [10] S. Delfino, A. Saccone, R. Ferro, *Z. Metallkde.* **71**, 165 (1980). Dariel, M., *Acta Crystallogr.* **20**, 586 (1966).
- [11] Y. Y. Chen, J. M. Lawrence, J. D. Thompson, J. O. Willis, *Phys. Rev. B* **40**, 10766 (1989).
- [12] H. H. Stadelmaier, T. S. Yun, *Z. Metallkde.* **52**, 477 (1961).
- [13] H. Haschke, H. Nowotny, F. Benosowsky, *Monatsh. Chem.* **97**, 1045 (1966).
- [14] R. Dronskowski, P. E. Blöchl, *J. Phys. Chem.* **97**, 8617 (1993).